A Novel 3D Imaging Methodfor Downward-Looking MIMO-SAR based onL_qRegularization

Le Kang[12],Li Sun[1], QunZhang[123], Tao-yongLi[12],Fu-fei Gu[4],Bi-shuai Liang[5]
[1]Information and Navigation College, Air Force Engineering University, Xi'an 710077, China
[2]Collaborative Innovation Center of Information Sensing and Understanding, Xi'an 710077, China
[3]Key Laboratory for Information Science of Electromagnetic Waves, Fudan University, Shanghai 200433, China
[4] China Satellite Maritime Tracking and Control Department, Jiangyin 214431, China
[5] Border Defense Academy of PLA, Xi'an 710108, China
E-mail: 18810495946@163.com

Abstract: Downward-looking multiple-input-multiple-output synthetic aperture radar (MIMO-SAR)three-dimensional (3D) imaging has wide application prospects. But to realize high cross-track resolution imaging needs lots of antenna elements and long antenna array, which are limited by the hardware. In this paper,a novelimaging methodfor downward-looking MIMO-SARbased onL_q regularization is proposed to solve this problem, which transforms the cross-track imaging processinto aL_q regularization modelby building and analyzing a structured over-complete dictionary based on the echo signal. With the proposed method, betterresolutioncan be obtained and a smaller amount ofantenna elementsis required for imaging compared to the conventional method. The proposed method has been verified by simulations.

Keywords: MIMO SAR;3D imaging;L_q regularization;

I. INTRODUCTION

Downward-looking multiple-input-multiple-output synthetic aperture radar (MIMO-SAR) three-dimensional (3D) imagingis an innovative imagingmode based on traditional twodimensional (2D)SAR and MIMOradar imaging, which obtains range resolution by pulse compression, azimuth resolution by virtual aperture synthesis withplatform movement, and cross-track resolution by a lineararray antenna[1]. Downward-looking 3D SAR can avoid the height ambiguity problem in SARtomography caused by the uneven track distribution and overcome shadingrestrictions [2]. Therefore, a 3D imaging radar for unmanned airplanes named ARTINO which can obtain exact 3D images was developed [3]. Klare studied the impact of platform attitude disturbances on the 3D imaging quality of the unmanned aerial vehicle (UAV) ARTINO and proposed the error correction method [4]. Since then, a number of traditional 2D SAR imaging algorithms and motion compensation methods were used in this 3D imagingmode like chirp scalingalgorithm and pseudopolar format algorithm, which can produce clear images and avoid the problem in the large amount of interpolations[5].

In recent years, with the development of technology, UAV is getting mature and has been used in all fields, especially in SAR imaging [6]. However, matched filtering (MF) based downward-looking MIMO-SAR 3D imaging methods arecomputationally efficient, but it may suffer from clutter, sidelobe andazimuth ambiguity, which restrict applications of the method[7]. A novel imaging algorithm based on compressive sensing (CS) preserves the super-resolution in cross-track domain [8]. However, the works utilize CS theory in the processing of imaging and focus on improving the quality of image, nevertheless, they don't provide effective means to settle the problem that theantenna elements are still too much for UAV.

In this paper,we propose anovel 3D imaging method for downward-looking MIMO SAR based on L_q regularization [9] to solve the problem that the antenna elements with high resolution imaging is too many for UAV. This method creatively builds a structured over-complete dictionarybased on analysing the echo signal, and transforms the processing of cross-track domain into a $L_q$regularization model which can be solved throughimprovedsparse Bayesian learning (SBL)[10]. While high resolution imaging and lower sidelobes to achieve high quality images, the proposed method decreases the number of antenna elements significantly.

II. ECHOSIGNAL PREPROCESSING

The geometry of downward-looking3D SAR is shown in Figure 1.x,y, and $z$respectively denote theazimuth, cross-track, and range domain. The radar platform flies along the x-axis corresponding toazimuth direction, with velocity v at height H. Suppose there are Nscatterers in the observed scene, and their coordinates are P_n= (x_n,y_n,z_n), n=1,2,…,N.

The antenna arrayis parallel to y-axis, whichcontains$N_t$transmitting antennaelements and$N_r$receiving antenna elements. tp, p=1,2,…,N_t denotes transmitting antenna elementsand the distance between eachtwo elements is 2d.rq, q=1,2,…,N_r denotes receiving antenna elements and the distance between two elements is N_t•d. Each time, only one transmitting antenna element transmits signal and all the receiving antenna elements receive echo simultaneously. The length of the antenna array is N_t•N_r•d[11].

According to the principle of equivalent phase center (EPC) [12], the phase error compensation function is:

$$H_1 = exp\left(j\pi \left(y_{tp} + y_{rq} \right)^2 / 2\lambda R_s \right) \quad (1)$$

wherey_{tp} denotes the position of the p-thtransmitting antennaelement, y_{rq} denotes the position of the q-threceiving antennaelement, λ is the wavelength and R_s=H.

Considering the problem that the equivalent antenna elementsare not in astraight line with the time division mode and the movement of the platform in the azimuthdirection, thephase compensation function of the equivalent antenna elements in i-th pulse repetition period is [7]:

This work was supported by the National Natural ScienceFoundation of China under Grant 61501498 and Grant 20151996016, Coordinator Innovative Engineering Project of Shaanxi Province under Grant 2015KTTSGY0406.

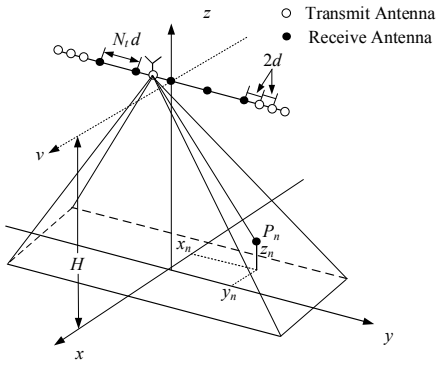

Fig. 1. Geometry of down-looking MIMO SAR.

$$H_2 = exp\left(j\pi \left(v(i-1)PRT \right)^2 / 2\lambda R_s \right) \quad (2)$$

The chirp signaltransmitted by *tp* is:

$$S_p(t) = rect\left(t / T_p\right) exp\left(j2\pi f_c t + j\pi K_r t^2\right) \quad (3)$$

where*t* is the fast-time, T_p is the duration time, f_c is the carrier frequency and K_r is the chirp rate.

The echo signal received by *rq*can be written as:

$$\begin{aligned} S_{pq}(t) = \sum_{n=1}^{N} \sigma_n rect\left(\frac{t - R_{tp,rq}/c}{T_p} \right) rect\left(\frac{x - x_n}{L_{sar}} \right) \\ \times exp\left(j\pi K_r \left(t - \frac{R_{tp,rq}}{c} \right)^2 \right) exp\left(j2\pi f_c \left(t - \frac{R_{tp,rq}}{c} \right) \right) \end{aligned} \quad (4)$$

whereσ_n is the reflectivity of *n*-thscatterer, L_{sar} is the length of synthetic aperture, *c* is the speed of light, $R_{tp,rq} = R_{tp,pn} + R_{pn,rq}$, $R_{tp,pn}$ is the distance between *tp* and P_n, $R_{pn,rq}$ is the distance between $P_n$and*rq*.

After doing equivalent phase error correction by (1) and doing motion correction by (2), the pre-processing is the same as the processing in traditional SAR imaging, which includes range compression, range cell migration correction (RCMC) and azimuth compression.

The echo signal after pre-processing can be expressed as:

$$\begin{aligned} S_{pq,c}(\hat{t}, t_m) = \sum_{n=1}^{N} \sigma_n sinc\left(B_r \left(\hat{t} - \frac{2R_e}{c} \right) \right) sinc\left(B_a \left(t_m - \frac{x_n}{c} \right) \right) \\ \times exp\left(j\frac{2\pi}{\lambda} \left(\frac{2y_n y_{pq}}{R_B} - \frac{{y_{pq}}^2}{R_B} \right) \right) exp\left(-j\frac{4\pi}{\lambda} R_{\boldsymbol{B}} \right) \end{aligned}$$

(5)where $R_e = R_B + \frac{{y_{pq}}^2}{2R_B} - \frac{2y_{pq}y_n}{2R_B}$ is the distancebetween the equivalent antennaelement and the point scatterer after RCMC, $R_B = \sqrt{\left(H - z_n\right)^2 + {y_n}^2}$ and B_a is the Doppler bandwidth.

III. L_Q REGULARIZATION MODEL

A. L_q Regularization Modeling

For digital signal processing, discretize (8) as follows:

$$S_{pq,cN_x \times N_z} = \left[\varphi_{pq,1}, \varphi_{pq,2}, \ldots, \varphi_{pq,n} \right]_{1 \times N} \left[\rho_1, \rho_2, \ldots, \rho_n \right]^T_{N \times (N_x \times N_z)} \quad (6)$$

where $\varphi_{pq,n} = exp\left(j2\pi \left(2y_n y_{pq} - {y_{pq}}^2 \right) / \left(\lambda R_B \right) \right)$,

$\rho_n = \sigma_n sinc\left(B_r \left(\hat{t} - \frac{2R_e}{c} \right) \right) sinc\left(B_a \left(t_m - \frac{x_n}{c} \right) \right) exp\left(-j\frac{4\pi}{\lambda} R_{\boldsymbol{B}} \right)$,

N_x is the number of the pulsars, N_z is the number of sampling points for each pulse,n_x=1,2,…,N_x and n_z=1,2,…,N_z. The equivalent antenna array can be rearranged as:

$$\hat{y} = \left[y_{11}, y_{12}, \ldots, y_{1Nr}, y_{21}, y_{22}, \ldots, y_{2Nr}, \ldots y_{Nt1}, y_{Nt2}, \ldots, y_{NtNr} \right] \quad (7)$$

The echo signal transmitted and received by all the equivalent antenna elements should be a 3D matrix:

$$\begin{aligned} S_c &= \left[S_{11,c}, S_{12,c}, \ldots, S_{1Nr,c}, S_{21,c}, S_{22,c}, \ldots, S_{2Nr,c}, \ldots, S_{Nt1,c}, S_{Nt2,c}, \ldots, S_{NtNr,c} \right]^T \\ &= \left[S_{1,c}, S_{2,c}, \ldots, S_{L,c} \right]^T_{L \times (N_x \times N_z)} \end{aligned} \quad (8)$$

where $L = N_t \times N_r$ denotes the number of the equivalent antennaelements.

Divide the cross-track imaging area $\left[-Y_0, Y_0 \right]$ by Δy interval, and the discretized positions can be expressed as:

$$y_{n_y} = -Y_0 + 2Y_0 \left(n_y - 1 \right) / L, \quad n_y = 1,2,\cdots, \quad N_y \quad (9)$$

where $N_y = 2Y_0 / \Delta y$.

Project $\rho_1, \rho_2, \cdots, \rho_N$ onto (9), which include the reflectivity ofscatterers. Then a sparse vector which denotes the imaging result can be given as:

$$\boldsymbol{\rho} = \left[\rho_1, \rho_2, \ldots, \rho_{Ny} \right]^T_{N_y \times (N_x \times N_z)} \quad (10)$$

where$\rho_i$is not equal to 0 if there is a point scatterer at y_i.

According to (6), (8) and (9), the over-complete dictionary can be given as

$$\boldsymbol{\Phi} = \begin{bmatrix} \varphi_{1,1}, & \varphi_{1,2}, \cdots, & \varphi_{1,N_y} \\ \varphi_{2,1}, & \varphi_{2,2}, \cdots, & \varphi_{2,N_y} \\ & \vdots & \\ \varphi_{L,1}, & \varphi_{L,2}, \cdots, & \varphi_{L,N_y} \end{bmatrix} \quad \varphi_{i,j} = exp\left(j\frac{2\pi}{\lambda} \left(\frac{2y_j \hat{y}_i}{R_B} - \frac{{\hat{y}_i}^2}{R_B} \right) \right) \quad (11)$$

In the more realistic case, adding on thenoise signal *e*, (6) can be written as

$$\mathbf{S}_{cL \times (N_x \times N_z)} = \boldsymbol{\Phi}_{L \times N_y} \boldsymbol{\rho}_{N_y \times (N_x \times N_z)} + e \quad (12)$$

Based on $L_q$regularization , (12) can be transformed into：

$$\boldsymbol{\rho}' = argmin\left\{ \left\| \mathbf{S}_c - \boldsymbol{\Phi}\boldsymbol{\rho} \right\|_2^2 + \boldsymbol{\lambda} \left\| \boldsymbol{\rho} \right\|_q \right\}, \quad 0 < q < 1 \quad (13)$$

where $\boldsymbol{\rho}'$ isthereconstructed scene and $\boldsymbol{\lambda}$ is the regularization parameter.

B. Solvability of the L_q RegularizationModel

Two conditions are needed in order to confirm the existence and uniqueness of the solution of (13). Firstly, the unknown

vector $\boldsymbol{\rho}$should be sparse which has been demonstrated by above analysis. Secondly, the dictionary matrix $\boldsymbol{\Phi}$should be satisfied with the restricted isometry property (RIP) [13].

However, confirming the RIP of $\boldsymbol{\Phi}$isa NP-hard problem, so a widely used method [14] based on point spread function (PSF) is as follows

$$PSF(m,\ n)=\langle \boldsymbol{\Phi}_m,\ \boldsymbol{\Phi}_n\rangle / \|\boldsymbol{\Phi}_m\|_2 \|\boldsymbol{\Phi}_n\|_2 \tag{14}$$

where$\boldsymbol{\Phi}_m$is the m-th column in $\boldsymbol{\Phi}$.

According to (14), $\|\Phi_m\|_2=1$. So (14) can be written as:

$$PSF(m,\ n)=\sum_{i=1}^{L}\varphi_{i,m}\varphi_{i,n}^{*}=\sum_{i=1}^{L}exp\left(j\frac{4\pi}{\lambda R_B}(y_n-y_m)\hat{y}_i\right) \tag{15}$$

In fact, if there is an integration instead of the summation in (15), the *PSF* will be a sinc function. So the PSF of $\boldsymbol{\Phi}$approximates to the identity matrix when the antenna array is long enough, which means the $\boldsymbol{\Phi}$is satisfied with RIP.

However, doing under-sampled is equal to the $\boldsymbol{\Phi}$and $\mathbf{S_c}$ left multiplied by sampling matrix $\mathbf{G}$: $\boldsymbol{\Phi}'=\mathbf{G}\boldsymbol{\Phi}$and $\mathbf{S_c}'=\mathbf{G}\mathbf{S_c}$, which will cause sidelobe distortion in the PSF of $\boldsymbol{\Phi}'$. So the RIP of $\boldsymbol{\Phi}'$depends on the under-sampledmatrix $\mathbf{G}$ of the antenna array.

The relationship between RIP of $\boldsymbol{\Phi}'$and the antenna array will be discussed with simulation results.

C. L_q Regularization Model Solving

Based on the improvedSBL[10], we can estimate$\boldsymbol{\rho}$as:

$$\begin{aligned}\boldsymbol{\rho}&=\arg\max_{\boldsymbol{\rho},\ \boldsymbol{\lambda},\ \beta}\left\{F(\boldsymbol{\rho},\ \boldsymbol{\lambda},\ \beta)=\log\ P(\boldsymbol{S}_c',\boldsymbol{\rho})\right\}\\&=\arg\max_{\boldsymbol{\rho},\ \boldsymbol{\lambda},\ \beta}\left\{F(\boldsymbol{\rho},\ \boldsymbol{\lambda},\ \beta)=-\frac{N_y}{2}\log\beta+\frac{\beta}{2}\|\boldsymbol{S}_c'-\boldsymbol{\Phi}'\boldsymbol{\rho}\|_2^2\right.\\&\qquad\left.+\frac{1}{q}\sum_{i=1}^{L}\left(\lambda_i|\rho_i|^q-\log\lambda_i\right)+C\right\}\end{aligned} \tag{16}$$

where$\beta^{-1}=\sigma_e^2$.

Take the derivative of (22), and the iterative formula is:

$$\begin{cases}\left(\beta^{-1}\right)^{(n+1)}=\left\|\boldsymbol{S}_c'-\boldsymbol{\Phi}'\boldsymbol{\rho}^{(n)}\right\|_2^2/N_y\\ \lambda_i^{(n+1)}=1/\left|\rho_i^{(n)}\right|^q;(i<L)\\ \boldsymbol{\rho}^{(n+1)}=\left(\boldsymbol{\Phi}'^{\mathrm{T}}\boldsymbol{\Phi}'\right)^{-1}\left(\boldsymbol{\Phi}'^{\mathrm{T}}\boldsymbol{S}_c'-\left(\boldsymbol{p}\beta^{(n)}\right)^{-1}\boldsymbol{V}^{(n)}\boldsymbol{\lambda}^{(n)}\right)\end{cases} \tag{17}$$

where $\boldsymbol{V}=diag(v_1,\cdots,v_L)$，$v_i=sign(\rho_i)$, $i=1,2,\ \cdots,L$.

So the specific steps are as follows:

- Initialize $\boldsymbol{\rho}^{(0)}$=0, δ, ε, and iterator k = 1;
- Calculate the parameter$\boldsymbol{\lambda}^{(k)}$, $\beta^{(k)}$ and update $\boldsymbol{\rho}^{(k)}$ by (17);
- Delete $\rho_i$and the $\boldsymbol{\Phi}'$ if $|\rho_i|$<δ;
- If$\left\|\boldsymbol{\rho}^{(k)}-\boldsymbol{\rho}^{(k-1)}\right\|_2/\left\|\boldsymbol{\rho}^{(k-1)}\right\|_2\geq\varepsilon$, set k=k+1 and return to the second step;
- Output 3D imaging result $\boldsymbol{\rho}$.

IV. Simulation Results

In this section, some simulationsareperformed to verifythe validity of the proposed imaging algorithm. The main parameters used for simulations are listed in Table I. In order to balance the imaging efficiency and quality, q in L_q is 1/2 in the following simulations [15].

Suppose that there are eight point scatterers located at thescene with the azimuth-range-cross track values equal to (10, 200, -2), (10, 200, 2), (20, 200, -2), (20, 200, 2), (10,190, -2), (10,190, 2), (20,190, -2), and (20,190, 2) respectively.The distributions of the eight pointscatterers are shown in Figure 2(a). After 3D imaging processing by using the proposed method,the surfaces of the final 3D image are plotted at −3 dB inFigure 2(b).The imaging results show that the point scatterers arewell focused in 3D space, confirming the validity of theproposed algorithm.

According to the definitions of the PSF and $\boldsymbol{\Phi}$, if the value of $PSF(m,n)$ is close to 0, the point scatterers at y_n and y_m can be distinguished.

When the antenna array is 1.68m,Figures3(a) and 3(b) respectively show the *PSF* of $\boldsymbol{\Phi}'$with full antenna elements and 1/4 Gaussian randomunder-sampled antenna elements. Figure 3(c) showsthe final 3D image in the same case with Figure 3(a).

Figure 3(a) confirms that PSF of $\boldsymbol{\Phi}$in (15) approximates to unit matrix when the length of array is 1.68m. Although stochasticsidelobes appear in Figure 3(b) as a result of the Gaussian randomunder-sampled matrix $\mathbf{G}$, it canbe seen that the *PSF of* $\boldsymbol{\Phi}'$ is much less than 1 when m is not equal to n. To a certain extent, the $\boldsymbol{\Phi}'$ is satisfied with RIP by the decreases of antenna elements.

Suppose that there are two point scatterers located at thescene with the azimuth-range-cross track unit of (10, 200, 0) and (10, 200, 0.15). In order to analyze the performance of the proposedmethod, the imaging result obtained by Fourier transformis given for comparison.Figure 3(e) shows the cross track reconstruction result obtained byFourier transform, andFigure 3(f) shows the cross track reconstruction resultobtained by the proposedmethod with 1/4 Gaussian randomunder-sampled antenna elements.As the cross-track distanceof the two targets is 0.15° , which is less than the cross-trackresolution of 0.27° , the two targets can not be distinguishedin the image obtained by Fourier based method. However,the proposed method with fewer antenna elements can improve the spatial resolution anddistinguish the two targets clearly.By comparing the imaging results, it canbe seen thatthe proposedmethodcan provide betterresolution and lower sidelobes.

V. Conclusions

In this paper, in order to reduce the number of antenna elements and obtain high resolution, we proposed a novel 3D imaging methodfor downward-looking MIMO SAR based on $L_q$regularization.The imaging processing is transformed into

TABLE I. PARAMETERS USED FOR SIMULATION

Parameters	Value	Parameters	Value
f_c(GHz)	37.5	bandwidthBr (MHz)	300
H(m)	200	v(m/s)	15
$T_p(\mu s)$	0.1	Azimuth aperture D(m)	0.8
L(m)	1.68	N_t	20
beamwidth θ (°)	10	N_r	21

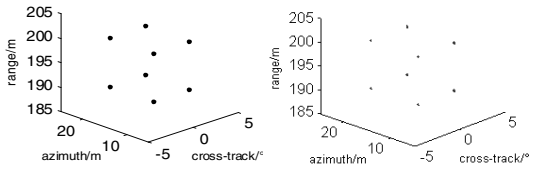

(a) Real spatial position (b) Final3D image

Fig. 2. image of the point scatterers.

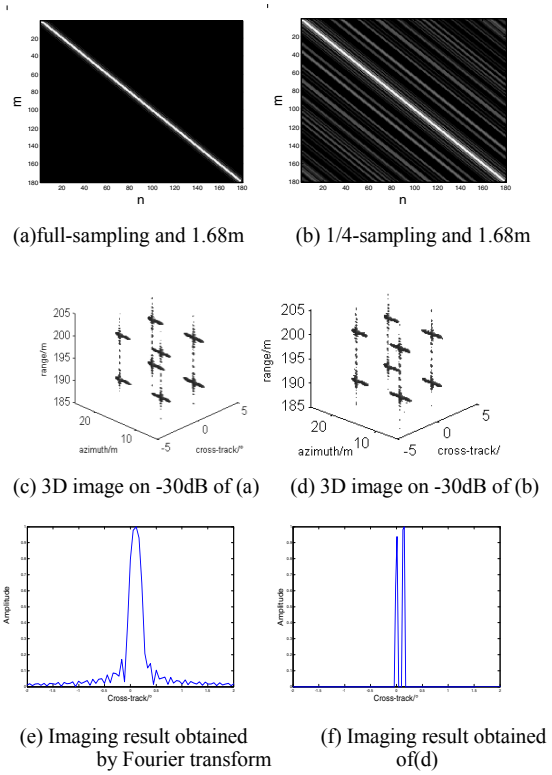

(a)full-sampling and 1.68m (b) 1/4-sampling and 1.68m

(c) 3D image on -30dB of (a) (d) 3D image on -30dB of (b)

(e) Imaging result obtained by Fourier transform (f) Imaging result obtained of(d)

Fig. 3. PSF of $\mathbf{\Phi}$ and $\bar{\mathbf{\Phi}}$.

aL_q regularization model by building the over-complete dictionary, which can be solved by SBL. Compared to the conventional method,the proposed method can provide betterresolution and lower sidelobes,or reduce the number of antenna elements significantly. However, the antenna optimization method and the impact of the micro-motion of antenna array need more investigation.

REFERENCES

[1] Klare, J., et al. "Image quality analysis of the vibrating sparse MIMO antenna array of the airborne 3D imaging radar ARTINO. " IEEE International Geoscience & Remote Sensing Symposium, IGARSS 2007, July 23-28, 2007, Barcelona, Spain, Proceedings 2007:5310 - 5314.

[2] Wencheng, Xie, Z. Xiaoling, and S. Jun. "MIMO antenna array design for airborne down-looking 3D imaging SAR." Signal Processing Systems (ICSPS), 2010 2nd International Conference on IEEE, 2010:V2-452-V2-456.

[3] Weib, Matthias, and J. H. G. Ender. "A 3D imaging radar for small unmanned airplanes - ARTINO." Radar Conference, 2005. EURAD 2005. European 2005:209-212.

[4] Klare, Jens, A. Brenner, and J. Ender. "Impact of Platform Attitude Disturbances on the 3D Imaging Quality of the UAV ARTINO." European Conference on Synthetic Aperture Radar 2008:1-4.

[5] Zhang, Donghao, and X. Zhang. "Downward-Looking 3-D linear array SAR imaging based on Chirp Scaling algorithm." Synthetic Aperture Radar, 2009. Apsar 2009. Asian-Pacific Conference on IEEE, 2009:1043 - 1046.

[6] Nex, Francesco, and F. Remondino. "UAV for 3D mapping applications: a review." Applied Geomatics 6.1(2014):1-15.

[7] Klare, J. "Digital Beamforming For A 3D MimoSar - Improvements Through Frequency And Waveform. Diversity." Geoscience and Remote Sensing Symposium, 2008. IGARSS 2008. IEEE International 2008:V - 17 - V - 20.

[8] Zhang, Siqian, et al. "Truncated SVD-Based Compressive Sensing for Downward-Looking Three-Dimensional SAR Imaging With Uniform/Nonuniform Linear Array." Geoscience & Remote Sensing Letters IEEE 12.9(2015):1853-1857.

[9] Tikhonov, A N. "Regularization of Incorrectly Posed Problems." Sov Math 4.1(1963):1624-1627.

[10] Jabbarian-Jahromi, Mohammad, et al. "Fast two-dimensional sparse Bayesian learning with application to pulse Doppler multiple-input–multiple-output radars." Iet Radar Sonar Navigation (2015).

[11] Klare, et al. "A New Airborne Radar for 3D Imaging - Simulation Study of ARTINO." (2006).

[12] Hou, Haiping, et al. "Research on equivalent-phase-center analysis approach of airborne downward-looking array SAR." Chinese Journal of Scientific Instrument (2010).

[13] Tsaig, Yaakov, and D. L. Donoho. "Compressed sensing." IEEE Trans. Inform. Theory 2006:1289--1306.

[14] Lustig, Michael, D. Donoho, and J. M. Pauly. "Sparse MRI: The application of compressed sensing for rapid MR imaging." Magnetic Resonance in Medicine 58.6(2007):1182-1195.

[15] Xu, Zongben, et al. "L-1/2 Regularization: A Thresholding Representation Theory and a Fast Solver." IEEE Transactions on Neural Networks & Learning Systems 23.7(2012):1013-27.